PCCP

PAPER

Cite this: *Phys. Chem. Chem. Phys.*, 2018, **20**, 10697

Gas phase ^{1}H NMR studies and kinetic modeling of dihydrogen isotope equilibration catalyzed by Ru-nanoparticles under normal conditions: dissociative *vs.* associative exchange†

Hans-Heinrich Limbach, *[a] Tal Pery,[a] Niels Rothermel,[b] Bruno Chaudret,[c] Torsten Gutmann[b] and Gerd Buntkowsky[b]

Received 17th November 2017,
Accepted 19th December 2017

DOI: 10.1039/c7cp07770j

rsc.li/pccp

The equilibration of H_2, HD and D_2 between the gas phase and surface hydrides of solid organic-ligand-stabilized Ru metal nanoparticles has been studied by gas phase ^{1}H NMR spectroscopy using closed NMR tubes as batch reactors at room temperature and 800 mbar. When two different nanoparticle systems, Ru/PVP (PVP ≡ polyvinylpyrrolidone) and Ru/HDA (HDA ≡ hexadecylamine) were exposed to D_2 gas, only the release of HD from the hydride containing surface could be detected in the initial stages of the reaction, but no H_2. In the case of Ru/HDA also the reverse experiment was performed where surface deuterated nanoparticles were exposed to H_2. In that case, the conversion of H_2 into gaseous HD was detected. In order to analyze the experimental kinetic and spectroscopic data, we explored two different mechanisms taking into account potential kinetic and equilibrium H/D isotope effects. Firstly, we explored the dissociative exchange mechanism consisting of dissociative adsorption of dihydrogen, fast hydride surface diffusion and associative desorption of dihydrogen. It is shown that if D_2 is the reaction partner, only H_2 will be released in the beginning of the reaction, and HD only in later reaction stages. The second mechanism, dubbed here associative exchange consists of the binding of dihydrogen to Ru surface atoms, followed by a H-transfer to or by H-exchange with an adjacent hydride site, and finally of the associative desorption of dihydrogen. In that case, in the exchange with D_2, only HD will be released in the beginning of the reaction. Our experimental results are not compatible with the dissociative exchange but can be explained in terms of the associative exchange. Whereas the former will dominate at low temperatures and pressures, the latter will prevail around room temperature and normal pressures where transition metal nanoparticles are generally used as reaction catalysts.

Introduction

The interaction of dihydrogen with transition metal surfaces has been intensively studied in the past decades.[1–3] It is now commonly accepted that in the case of clean and ordered surfaces at low temperatures and pressures dihydrogen is subject to dissociative adsorption leading to surface hydrides.[2] The process requires at least two, possibly more clustered vacancies[4] and involves a barrier for dissociation. Rapid hydrogen diffusion or quantum delocalization between vacancies can occur[2,5] before the reverse associative desorption takes place. The kinetics of the latter have been studied using temperature programmed desorption (TPD) techniques;[2] no major differences were observed for H_2, HD and D_2.[6] To our knowledge, only in one case it was reported by Christmann *et al.*[7] that surface hydrides and non-dissociated molecular dihydrogen can sometimes coexist, for example on single crystal Pd surfaces.

In recent years, interactions of large transition metal clusters with hydrogen have become a focus of interest, either in the form of isolated molecules in the gas phase[8,9] or as deposits on solid scaffolds.[10] Surprisingly, it was observed for negatively charged Ru clusters in the gas phase that when all free hydride sites are occupied, massive associative adsorption of additional dihydrogen to free Ru atoms occurs[9] in a similar way as has been proposed before.[7,11] On the other hand, supported metal nanoparticles are useful catalysts for heterogeneous reactions.[12–14]

Solid metal nanoparticles or colloids with diameters of 1–100 nm have also been used to catalyze hydrogenations or other reactions, most often at normal pressures, temperatures

[a] *Institut für Chemie und Biochemie, Freie Universität Berlin, Takustr. 3, D-14195 Berlin, Germany. E-mail: limbach@chemie.fu-berlin.de*
[b] *Eduard-Zintl-Institut für Anorganische und Physikalische Chemie, Technische Universität Darmstadt, Alarich-Weiss-Str. 8, D-64287 Darmstadt, Germany*
[c] *Laboratoire de Physique et Chimie des Nano Objets, LPCNO, Institut National des Sciences Appliquées, 135 Avenue de Rangueil, Toulouse 31077, France*

† Electronic supplementary information (ESI) available. See DOI: 10.1039/c7cp07770j

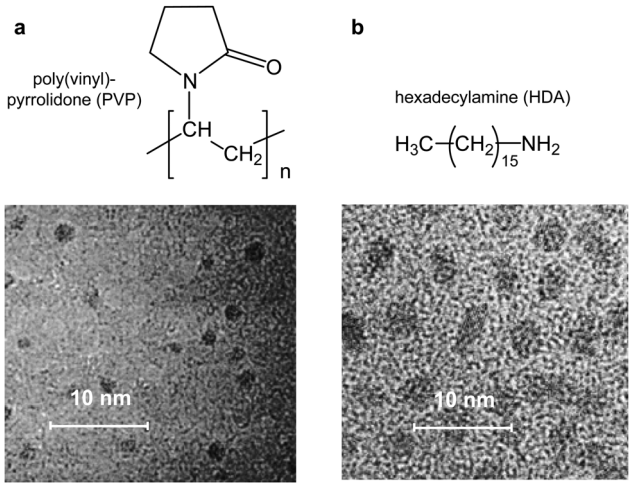

Fig. 1 Transmission electron micrographs of ruthenium nanoparticles in polyvinylpyrrolidone (PVP) and in hexadecylamine (HDA). Adapted from ref. 22.

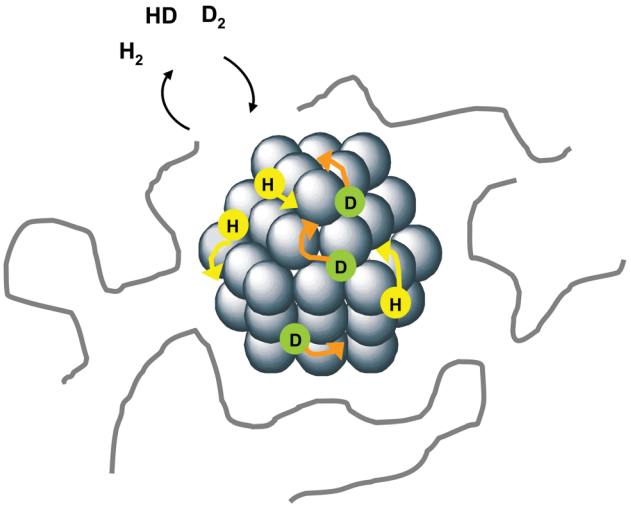

Fig. 2 Gas-surface exchange and equilibration of dihydrogen isotopes according to ref. 24.

and in the presence of solvents.[15–19] Such nanoparticles consist of an inner core of metal atoms embedded in and stabilized by organic ligands, either functionalized molecules or polymers.[20–22] In the transmission electron micrographs of the Ru nanoparticles of interest in this work, *i.e.* Ru/poly(vinyl)-pyrrolidone (Ru/PVP) and Ru/hexadecylamine (Ru/HDA), depicted in Fig. 1, the Ru-clusters appear as dark dots. For the Ru/HDA sample, the concentration and size of the clusters are larger than in Ru/PVP. Whereas PVP is supposed to constitute a weakly interacting ligand for surface Ru atoms, amino group containing compounds such as HDA are supposed to be bond more strongly to the Ru-surface *via* their nitrogen atoms.[23]

In contrast to clean metal surfaces, little is known about hydrogen or hydride species which constitute "active" partners of the catalytic behavior of metal nanoparticles. Previously, some of us have shown by ^{1}H gas phase NMR that freshly synthesized solid RuHDA nanoparticles release dihydrogen isotopologues in the minute time scale when they are exposed to gaseous D_2 as illustrated schematically in Fig. 2, indicating in this way the presence of surface hydrogen species.[24] Using solid state ^{2}H NMR it was then demonstrated that the deuterons bind to the Ru surface where they jump rapidly between different hydrogen sites around the particles. Their motion can be frozen at low temperatures. Moreover, some methylene groups of the HDA ligands are partially deuterated as a consequence of intermediate binding to the surface followed by H/D exchange.[25] Further ^{2}H solid state NMR[26,27] and computational studies[11,28] of Ru-nanoparticles and model systems demonstrated not only the occurrence of surface hydrides of the terminal RuH, bridging Ru(μ^2-H) and bridging Ru(μ^3-H) type but also of surface Ru(η^2-H_2/HD/D_2) dihydrogen complexes. The latter should be subject to rotational H_2[29] or D_2 tunneling.[30]

In order to elucidate further the interactions of dihydrogen with Ru-nanoparticles we decided to study the equilibration of gaseous dihydrogen isotopologues catalyzed by Ru/PVP and Ru/HDA in more detail. The idea which we pursued is illustrated in Fig. 3. When D_2 gas is brought in contact with Ru nanoparticle surfaces containing surface hydrides (Fig. 3a) one can discuss two different reaction mechanisms by which the isotopic equilibria in the gas phase

$$H_2 + D_2 \rightleftarrows 2HD \quad (1)$$

as well as between the gas phase and the metal surfaces are established. The traditional dissociative exchange mechanism consists of the following steps: dissociative adsorption (Fig. 3b), rapid surface diffusion (Fig. 3c) and associative desorption (Fig. 3d). In this mechanism, in the early reaction stages only H_2 will be released (Fig. 3d). Based on the previous studies which demonstrated the possibility of surface dihydrogen complexes M(η^2-H_2)[7,9,11] we propose here a second mechanism, the associative exchange mechanism. In the latter, D_2 is bound by associative adsorption as dihydrogen moiety M(η^2-H_2) (Fig. 3e). This moiety may transfer a deuteron to an adjacent surface hydride, forming a M(η^2-HD)-moiety (Fig. 3f). In that case, no H_2, but only HD will be released in the very early stages of the reaction (Fig. 3g).

The main goal of this work was, therefore, to find a way in order to distinguish between both mechanisms. We realized soon that for that purpose we could not use traditional techniques of heterogenous catalysis where a gas stream of a H_2/D_2 mixture flows through a reactor containing a bed of a catalyst and where the outcoming gas stream is analyzed using mass spectroscopy in order to determine the ratio of H_2, D_2 and of the HD produced. Under these experimental conditions the number of surface hydrogens is negligible as compared to the atoms present in gas phase.[13] However, we thought that we might be able to distinguish both mechanisms if we could study the equilibration of hydrogen isotopologues under conditions of comparable concentrations of surface hydrogen and gaseous hydrogen atoms.

Therefore, we explored in our work gas phase ^{1}H NMR which allows one to study sealed NMR sample tubes equipped with a

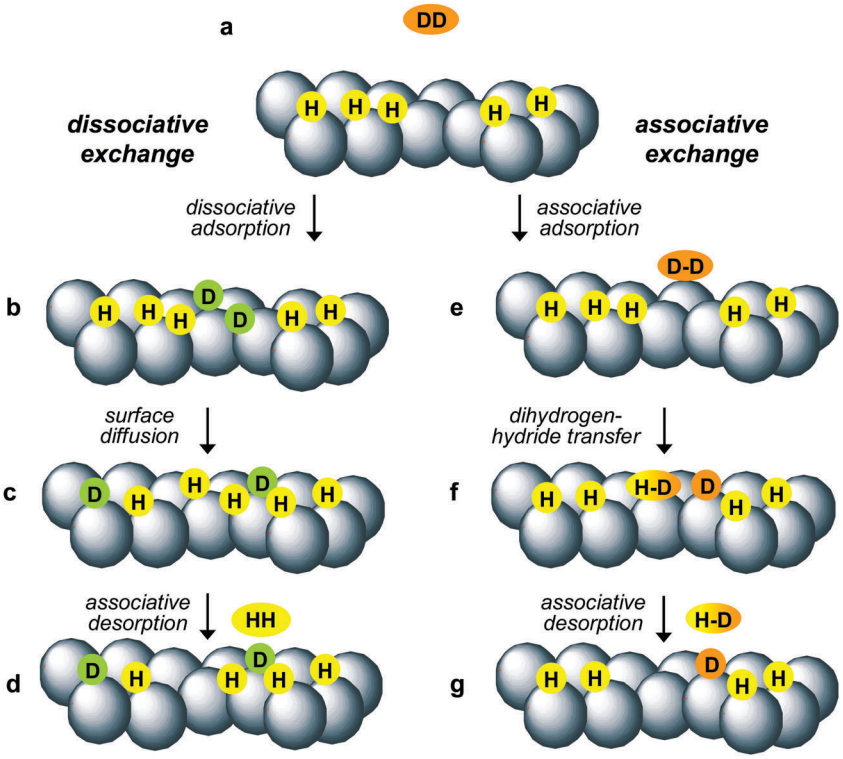

Fig. 3 Mechanisms (schematically) of equilibration of gaseous dihydrogen isotopes in contact with a catalyzing transition metal surface. Left side: Dissociative exchange model consisting of dissociative adsorption, surface diffusion, and associative desorption operative at low temperatures and low pressures. For details of each step see ref. 3. Right side: Associative exchange model proposed in this work, consisting of associative adsorption and formation of a surface dihydrogen complex followed by dihydrogen–hydride transfer and associative desorption. When D_2 interacts with a hydrogen containing surface H_2 is preferentially formed initially in the dissociative exchange whereas HD is preferentially formed in the associative exchange.

teflon needle valve.[31] Inside such a tube one can place solid catalysts in sufficient quantity as well as a relatively small quantity of gases around 1 bar. Gas phase ^{1}H NMR is especially useful to study H_2 and HD as they can be distinguished because of their different longitudinal and transverse relaxation *i.e.* different line width.[32] In this work, we studied two types of Ru-nanoparticles *i.e.* Ru/hexadecylamine (HDA) and Ru/polyvinylpyrrolidone (PVP).

As we were not aware of a similar equilibration study of a closed dihydrogen/metal system, we needed to derive differential equations suitable to simulate the time dependence of the concentrations of the dihydrogen isotopes in the gas phase for both mechanisms depicted in Fig. 3. Thus, we considered both the dissociative as well as the associative exchange mechanism, and took potential kinetic and equilibrium isotope effects into account, in particular the non-statistical distribution of dihydrogen isotopes H_2, HD and D_2 in the gas phase.

This paper is organized as follows. After an experimental section we explain in a theoretical section shortly the main ideas how to treat the reaction models depicted in Fig. 3 from a kinetic standpoint. The kinetic equations are assembled in the Appendix, and a full derivation of all equations is included in the ESI.† The formalism developed is used to describe the experimentally obtained concentrations of H_2, HD and D_2 in the gas phase at 800 mbar and room temperature over solid Ru nanoparticles as a function of time. The experimental results obtained for Ru/hexadecylamine (HDA) and Ru/polyvinylpyrrolidone (PVP) nanoparticles are then discussed. As shown below, we find evidence that the associative exchange mechanism is realized under normal conditions, which is important for the function of transition metal nanoparticles as catalysts for hydrogenation reactions under real conditions.

Experimental section

Synthesis of ruthenium nanoparticles

Ruthenium nanoparticles were prepared according to the procedure described by Pan *et al.*[22]

Ru/HDA

150 mg (0.50 mmol) of Ru(COD)(COT) were introduced into a Fischer–Porter bottle and left in vacuum during 30 minutes. 150 mL of THF degassed by three freeze–pump cycles were then added. The resulting yellow solution was cooled to 193 K after which a solution containing 0.10 mmol HDA in 25 mL THF was introduced to the flask. The bottle was pressurized with 3 bar dihydrogen and the solution was allowed to warm up slowly to room temperature. After 20 hours, a homogeneous brown solution is obtained. After elimination of excess dihydrogen, approximately 3 mL of the solution were passed under argon over a small alumina column. The absence of color of the

filtrate indicates the full decomposition of the precursor. The volume of the solution was then reduced to approx. 15 mL. 50 mL pentane were then added and the resulting mixture was cooled to 193 K at which temperature a brown precipitate formed. It was filtered, washed with pentane and dried in vacuum.

Ru/PVP

158 mg of Ru(COD)(COT) were placed into a Fischer–Porter bottle and left in vacuum during 30 minutes. Then, a solution of 1 g of PVP in 60 mL of THF, degassed by freeze–pump cycles was added. The resulting yellow solution was stirred for 30 min at room temperature. The bottle was pressurized at 3 bar dihydrogen and the solution was allowed to react for 68 hours, during which time a black precipitate formed. After elimination of excess dihydrogen, the solution was filtered and the black precipitate dried in vacuum. The precipitate was then re-dissolved in 30 mL of methanol, and the resulting solution was filtered and reduced to 15 mL. Addition of 30 mL of pentane led to a dark brown precipitate. It was filtered, washed with pentane and dried in vacuum.

Sample preparation

For gas phase NMR measurements, the purified and dry nanoparticles were placed at the bottom inside an empty NMR tube equipped with a teflon needle valve. For that operation a glove box was employed. The tube was then closed, attached to a vacuum line (outside the glove-box) equipped with a turbo molecular pump and then evacuated at 10^{-6} bar and 298 K. Finally, the NMR tube was filled with 800 mbar of H_2 or D_2 gas, closed and loaded into the NMR spectrometer and the ^{1}H NMR spectra of the gas phase above the nanoparticles were recorded.

NMR measurements

^{1}H gas phase NMR spectra (500.13 MHz) were recorded on a Bruker AMX 500 NMR spectrometer operating in the Fourier transform mode at a magnetic field of 11.7 T.

Theoretical section

In this section we present kinetic equations describing the equilibration of hydrogen isotopes in a closed system between the gas phase and a solid adsorbent such as metal nanoparticles containing atomic hydrogen binding sites, also called surface hydrides. We consider the high-pressure limit where the number N of dihydrogen isotopologues in the gas phase is independent of time, as well as the number of surface hydrogen isotopes. However, we are interested in the way of how the isotopic equilibrium between the gas phase and the surface is achieved, for example in the case where pure D_2 gas is let to interact with surface H, leading to an increase of HD and H_2 in the gas phase and to surface D in the adsorbent. In that process, besides the occurrence of kinetic H/D isotope effects, we take into account a potential isotope fractionation between surface and gas phase, as well as the well-established non-statistical distribution of dihydrogen isotopes in the gas phase (eqn (1)) which is characterized by the equilibrium constant

$$K_{\text{gas}} = \frac{n_{\text{HD}} n_{\text{HD}}}{n_{\text{H}_2} n_{\text{D}_2}} = 3.25 \text{ at room temperature.} \quad (2)$$

This value, calculated using isotope theory[33] and confirmed experimentally[34] means that at equilibrium there is less HD in the gas phase than expected for a statistical distribution where $K = 4$. We assume that diffusion in the gas phase is fast and does not constitute the rate limiting step.

As mentioned above, we consider two different reaction pathways which were illustrated in Fig. 3, *i.e.* a dissociative and an associative exchange of dihydrogen isotopes with transition metal surface hydrogen or hydride sites.

Unfortunately, it is difficult to treat theoretically and experimentally all reaction steps in Fig. 3. Therefore, we simplified the reactions in the following way.

For the dissociative exchange of dihydrogen isotopologues with hydrides on the metal nanoparticle surfaces we consider the following dissociative adsorption/associative adsorption steps

$$H_2 + 2^* \underset{k_d^{HH}}{\overset{k_a^{HH}}{\rightleftharpoons}} 2H^* \quad (3a)$$

$$HD + 2^* \underset{k_d^{HD}}{\overset{k_a^{HD}}{\rightleftharpoons}} H^* + D^*, \quad (3b)$$

$$D_2 + 2^* \underset{k_d^{DD}}{\overset{k_a^{DD}}{\rightleftharpoons}} 2D^*. \quad (3c)$$

According to the usual nomenclature of surface science as described by Chorkendorff *et al.*[35] an asterisk * indicates an unoccupied "atomic" binding site, whereas L* = H* or D* indicates any type of a hydrogen or deuterium bound surface site. The term 2* symbolizes two unoccupied binding sites. k_a^{LL} and k_d^{LL} represent the rate constants of adsorption and desorption of the dihydrogen isotope LL. The assumption of fast diffusion of hydrogen in the metal surfaces is taken into account by assuming that desorption of a given isotopologue is governed by the surface deuterium fraction.

In this model, we assume that gaseous dihydrogen molecules can bind to the surface and exchange directly hydrogen isotopes with a neighboring bound hydrogen, releasing again a dihydrogen molecule as illustrated in Fig. 3b.

For the associative exchange of dihydrogen isotopologues with hydrides on the metal nanoparticle surfaces we consider the following overall reactions,

$$H_2 + D^* \xrightarrow{k_e^{HHD}} H^* + HD, \quad (4a)$$

$$HD + D^* \xrightarrow{k_e^{HDD}} H^* + D_2, \quad (4b)$$

$$DH + H^* \xrightarrow{k_e^{DHH}} D^* + H_2, \quad (4c)$$

$$D_2 + H^* \xrightarrow{k_e^{DDH}} D^* + DH, \quad (4d)$$

The first two superscripts of the rate constants k_e^{LLL} stand for the reacting dihydrogen isotopologue and the last superscript for the surface bound hydrogen with which the exchange occurs. The following reactions will also be present

$$H_2 + H^* \xrightarrow{k_e^{HHH}} H^* + H_2, \quad (5a)$$

$$HD + H^* \xrightarrow{k_e^{HDH}} H^* + HD, \quad (5b)$$

$$HD + H^* \xrightarrow{k_e^{HDH}} H^* + DH, \quad (5c)$$

$$D_2 + D^* \xrightarrow{k_e^{DDD}} D^* + D_2, \quad (5d)$$

but they are not further considered here as they do not alter the concentrations of the isotopic species.

The main features and results of the kinetic treatment of both mechanism is presented in the Appendix. For interested readers we also present the full derivation in the ESI.†

Results

^{1}H gas phase NMR experiments of HH/HD mixtures

In contrast to H_2 in solution, gaseous H_2 gives rise to a broad NMR line because of short transverse relaxation times.[32] The line widths depend on pressure, temperature and the magnetic field used. Generally, increasing these variables decreases the line widths. At 500 MHz, 298 K and a pressure of about 1 bar, also the longitudinal relaxation times T_1 are short and of the order of 15 ms.[36] To our knowledge, no systematic T_2 study of hydrogen as a function of pressure, temperature and magnetic field has been reported.

We performed all NMR experiments at 500 MHz, a total pressure of 800 mbar, a temperature of 298 K, using the same recording parameters. Firstly, we performed NMR experiments on gaseous samples of H_2 and HD and on isotopic gas mixtures at 800 mbar total pressure. As shown in Fig. 4a and b, Lorentzian lines are observed for both isotopic species using 90° pulses, leading to the following expressions.

$$I_{H_2} = I_{H_2}(0)\frac{\pi W_{H_2}}{(\pi W_{H_2})^2 + 4\pi^2(\nu_{H_2} - \nu)^2}, \quad W_{H_2} = 1400 \text{ Hz},$$
$$\nu_{H_2} = 2250 \pm 100 \text{ Hz}, \quad \delta_{H_2} = 4.5 \pm 0.2 \text{ ppm}, \quad (6)$$

$$I_{HD} = I_{HD}(0)\frac{\pi W_{HD}}{(\pi W_{HD})^2 + 4\pi^2(\nu_{HD} - \nu)^2}, \quad W_{HD} = 250 \text{ Hz},$$
$$\nu_{HD} = 2150 \pm 50 \text{ Hz}, \quad \delta_{HD} = 4.3 \pm 0.1 \text{ ppm} \quad (7)$$

Here, $I_{H_2}(0) = \frac{n_{H_2}}{Z}$ and $I_{HD}(0) = \frac{n_{HD}}{Z}$ represent the integrated signal intensities of H_2 and HD. The constant Z was determined before using a reference sample of pure HD at 550 mbar in a known volume of 2 cm^3 at 298 K whose signal intensity was set to the reference value $I_{HD}(\text{ref}) = 1$, therefore,

$$Z = n_{HD}(\text{ref}) = \frac{pV}{RT} = \frac{0.55 \times 0.002}{0.08314 \times 1000 \times 298}\left[\frac{\text{bar} \times \text{L}}{\text{L} \times \text{bar K}^{-1}\ \text{mmol}^{-1} \times \text{K}}\right] = 0.044\underline{4}\ \text{mmol} \quad (8)$$

The reference sample was measured in each kinetic run of a given sample in order to calibrate its signal intensities in terms of number of molecules.

Fig. 4c shows the ^{1}H gas phase spectrum of a gas mixture containing 100 mbar H_2 and 700 mbar HD. The broad component arising from H_2 is barely visible, but can be detected by line shape analysis after performing a proper base-line correction. We checked the amount of H_2 by ^{1}H NMR after transfer into $CDCl_3$ (Fig. 4d); because of the much smaller line width, the correct H_2/HD ratio of 1 : 3.5 is now obtained. Therefore, in order to measure the amounts of H_2 and HD by gas phase ^{1}H NMR it was necessary to perform line shape analyses in terms of the sum of eqn (6) and (7), where only $I_{H_2}(0)$ and $I_{HD}(0)$ were varied. This procedure works well in the presence of large amounts of H_2 as shown later. However, in cases of spectra

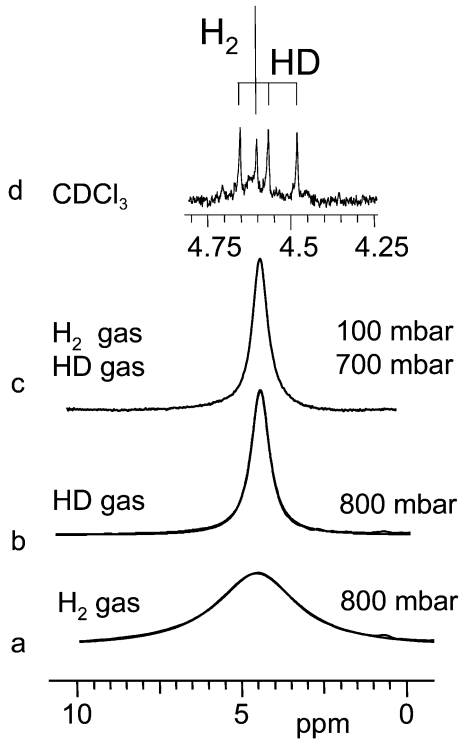

Fig. 4 500 MHz ^{1}H NMR spectra of different gas samples: (a) gas phase ^{1}H NMR spectrum of a sample containing 800 mbar H_2 gas. (b) Gas phase ^{1}H NMR spectrum of a sample containing 800 mbar HD gas. (c) Gas phase ^{1}H NMR spectrum of a sample containing a mixture of 100 mbar H_2 and 700 mbar HD gas. (d) Liquid state ^{1}H NMR spectrum of a gas mixture of 100 mbar H_2 and 700 mbar HD transferred into $CDCl_3$.

such as depicted in Fig. 4c, where HD dominates, base line distortions make it difficult to determine $I_{H_2}(0)$. In these cases we determined only the amount of $I_{HD}(0)$ by line shape analysis using eqn (7), using a base line correction which included the contribution of the H_2 signal.

We checked whether a spin–echo sequence, 90°–τ–180°–τ–echo,[37] could help to improve the method. However, although the base line distortions were minimized using τ values larger than 20 μs, H_2 signal intensity losses occurred because of its short T_2. Therefore, this method was not used further.

^{1}H gas phase NMR equilibration studies of gaseous dihydrogen isotopes in contact with Ru/HDA and Ru/PVP nanoparticles

In the early stages of our study we placed some of the powdered Ru/HDA nanoparticles at the bottom of NMR tubes equipped with a teflon needle valve, evacuated the sample to 10^{-6} bar and closed the valve. When we left the sample for several hours at 298 K we could not observe a pressure increase arising from thermally desorbed H_2. Even after heating the sample to 360 K for one day no pressure increase was observed. Later, we found that the Ru/HDA samples still contained surface hydrogen.

As has been described previously,[24] in order to detect its amount, we filled NMR tubes containing powdered Ru/HDA nanoparticles after extended evacuation *in vacuo* with 800 mbar D_2 gas at room temperature, inserted the samples into the NMR spectrometer, and measured the ^{1}H gas phase spectra at different reaction times. We observed a new peak around 4.5 ppm which grew with time. When we measured the solid state ^{2}H NMR spectra of the nanoparticles[24] we found two types of ^{2}H signals, a sharp signal which we assigned to mobile deuterons in the nanoparticle surface, and a broad signal typical for more or less rigid C–D units. The amount of the latter increased substantially when D_2 gas was added just after the synthesis of Ru/HDA and exposure to D_2 gas for several days. These results were corroborated by temperature-dependent solid state ^{2}H NMR measurements. Therefore, we concentrated in this study on the kinetics of the H/D gas-surface exchange as described in the following.

We prepared again Ru/HDA nanoparticles, inserted them into NMR sample tubes containing teflon needle valves, evacuated the samples, and added 800 mbar D_2 at room temperature. Then we transferred a given sample into the NMR spectrometer and measured the ^{1}H NMR gas phase spectra as a function of time. We dub this sample as Ru/HDA/H + D_2 sample. Unfortunately, as the chemical laboratory and the NMR laboratory were not closely located to each other, the dead time between the start of the reaction in the chemical laboratory and the beginning of the NMR measurements was almost 10 minutes.

Some typical superimposed experimental and calculated spectra obtained for the Ru/HDA/H + D_2 sample as a function of the time after the start of the reaction are depicted in Fig. 5, including a spectrum of the empty tube (top). The spectra were simulated as sums of the empty tube spectrum and the Lorentzian lines of H_2 and HD as given by eqn (6) and (7). Within the margin of error, no contribution from H_2 could clearly be observed, but only the appearance of HD as illustrated in Fig. 5. After a substantial increase within the first hour, the HD signal growth became very small.

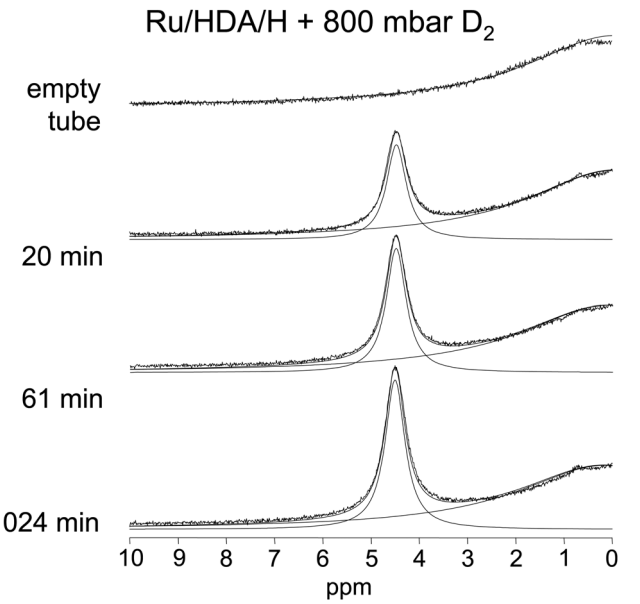

Fig. 5 Gas phase 500 MHz ^{1}H NMR spectra of a Ru/HDA/D + H_2 sample (800 mbar D_2) inside a closed NMR glass tube showing the release of HD at different reaction times.

In a second stage, we wanted to know whether the deuterons incorporated into the particles could be replaced again by hydrogen. For that purpose, a (partially) deuterated sample, dubbed as Ru/HDA/D + H_2 sample, was exposed to 800 mbar H_2 gas and the ^{1}H gas phase NMR spectra of this sample recorded again at different reaction times. Some typical spectra obtained are depicted in Fig. 6. Now, the broad H_2 signal could clearly be observed as major signal component, and the production of HD is demonstrated by the appearance of the sharper HD peak which increased with time at the expense of the H_2 signal. By line shape analysis using eqn (6) and (7), taking into account the spectrum of the empty NMR tube, the relative signal intensities of H_2 and HD could be determined.

In order to elucidate the influence of the stabilizing ligand we exposed a Ru/PVP sample to 800 mbar D_2 gas and measured the resulting ^{1}H gas phase NMR spectra at different reaction times. As a result, we obtained for this Ru/PVP/H + D_2 sample a similar increase of the gas phase HD peak around 4.5 ppm as in the case of Ru/HDA/H + D_2 sample.

Analysis of the kinetics of H/D exchange with Ru/HDA and Ru/PVP

By comparison of the ^{1}H signal intensities I obtained in the kinetic runs by line shape simulation with those of the reference sample (see Experimental section) we obtained the experimental time-dependent gas phase concentrations of the dihydrogen isotopologues as shown in Fig. 7 and 8. For convenience,

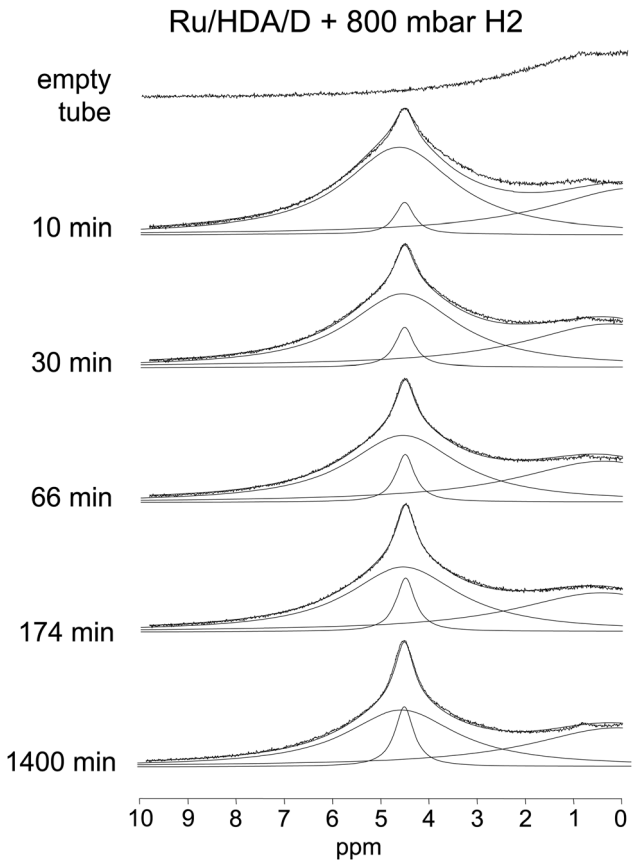

Fig. 6 Gas phase 500 MHz ^{1}H NMR spectra of a partially deuterated Ru/HDA/D + H_2 sample (800 mbar H_2) inside a closed NMR glass tube showing the conversion H_2 into HD as a function of time.

the concentrations were expressed in units of $Z = 0.049$ mmol. Each kinetic run was analyzed in terms of both the dissociative exchange model using eqn (15) and the associative exchange model using (23). Using home-made MATLAB programs the data were fitted to numerical solutions of these equations as described in the Appendix and the ESI.† The parameters used to simulate the experimental data are assembled in Table 1 for the dissociative and in Table 2 for the associative exchange model. We note that after calibration the signal intensities are given by $I_{HH} = 2x_{HH}$, $I_{HD} = x_{HD}$ and $I_{DD} = 2x_{DD}$. In Fig. 7 and 8, for a better comparison of the signal intensities, we always plotted I_{HH}, I_{HD} and $I_{DD}/2$. Moreover, on the left sides of Fig. 7 and 8 a linear scale for the reaction time is used, whereas on the right sides a logarithmic scale is used. These results will be discussed in detail in the following section.

Discussion

In this section, we will discuss how the experimental results described in the previous section will contribute to the question raised in Fig. 3 of whether the hydrogen isotope gas-surface equilibrium is better described in terms of the dissociative exchange model or of the associative exchange model.

Gas-surface hydrogen isotope equilibration over Ru nanoparticles: dissociative *vs.* associative hydrogen isotope exchange?

Let us firstly discuss the dissociative exchange model which was used in Fig. 7a and b to calculate the solid curve in order to reproduce the kinetic data of the Ru/PVP/H + D_2 sample and in Fig. 8a and b of the Ru/HDA/H + D_2 sample. Clearly, this model predicts that when Ru/HDA/H nanoparticles are treated with gaseous D_2, only H_2 is released in the beginning of the reaction which should lead to the dominance of the broad H_2 signal. That is because in this model fast surface diffusion is assumed with the consequence that for a given hydrogen the reaction partner H or D depends on their respective probability in the surface. As in the beginning of the reaction there is no D in the surface, no HD but only H_2 can be released. That is more than the H_2 equilibrium concentration, and hence the dissociative exchange model predicts that the H_2 signal intensity will go through a maximum and decrease again. At longer reaction times the HD signal will appear more slowly, even in the absence of kinetic isotope effects. In a qualitative way, this circumstance is already predicted by the simple schematic reaction scenario which was illustrated in Fig. 3. Only a small amount of D_2 is predicted to be released because of the overall small deuterium fraction in the system; again, in the beginning of the reaction more D_2 molecules are released as compared to the equilibrium.

As was illustrated in Fig. 5 for the Ru/HDA/H + D_2 sample, we could detect only the release of HD when Ru nanoparticles were treated with D_2. We could not exclude the formation of some H_2 whose broad signal might disappear in the base line. However, we did not observe spectra of the type depicted in Fig. 6 containing larger quantities of H_2, but that was predicted when we used the dissociative exchange model to reproduce the experimental HD signal intensities, those of H_2 being experimentally undetermined but small. Although we could simulate the results of the HDA/D + H_2 sample fairly well (Fig. 8c and d) we conclude, therefore, that the dissociative exchange model is not able to accommodate the kinetic data of the deuteration of the Ru nanoparticles.

By contrast, we could reproduce very well the experimental data of the Ru/PVP/H + D_2 and Ru/HDA/H + D_2 samples by using the associative exchange model (Fig. 3 and eqn (4)) as illustrated in Fig. 7c, d and 9a, b. That model predicts that after associative adsorption of D_2 followed by a dihydrogen-hydride transfer dominantly HD is released. H_2 is released only after longer reaction times. Thus, the calculated H_2 signal intensities are always much smaller than the HD signal intensities. Also, a good agreement between experimental and calculated data could be obtained for the reverse experiment, *i.e.* the Ru/HDA/D + H_2 sample as illustrated in Fig. 9c and d. We note that we needed to include the presence of some HD in the beginning of the reaction, as illustrated in Fig. 9c by the value of the HD intensity at $t = 0$. We associate this finding to the presence of some very reactive sites of the type Ru(η^2-HD) in Ru/HDA/D. Similar sites of the type Ru(η^2-DD) might also be present but a fast DD release can not be detected by ^{1}H NMR. In the case of Ru/HDA/H, Ru(η^2-HH) might be present, but the fast release of a small number of H_2 is difficult to be detected.

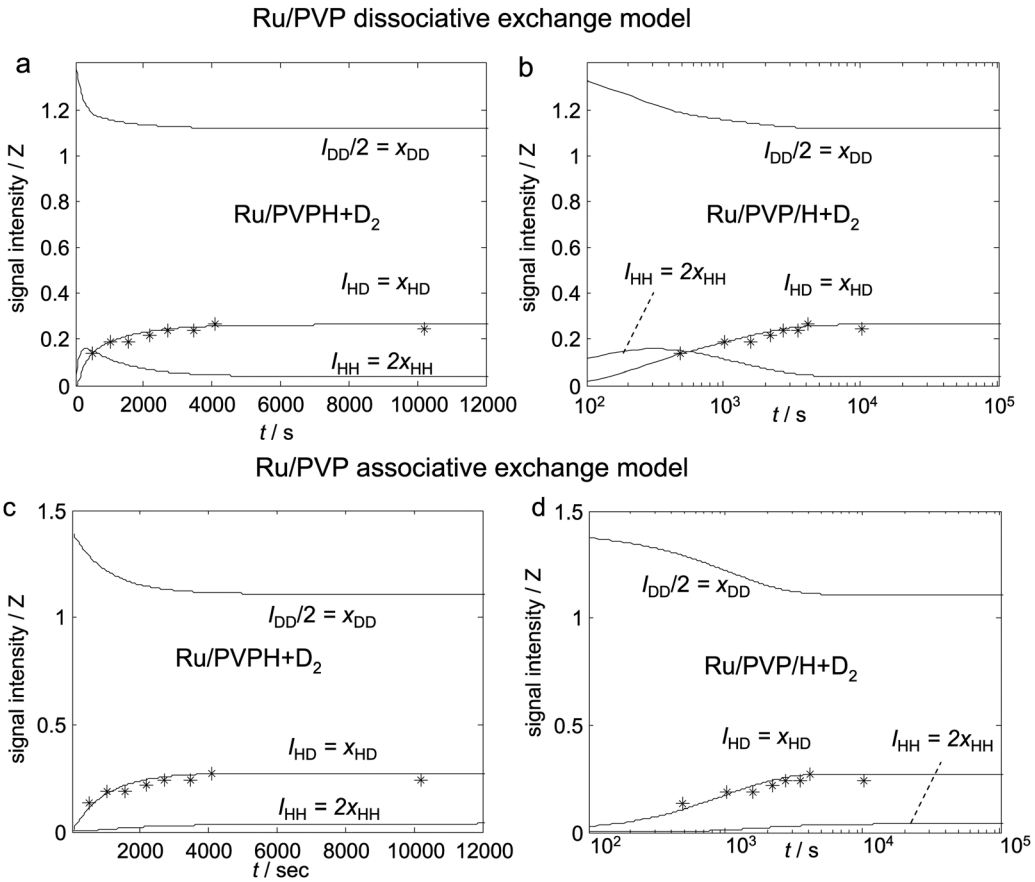

Fig. 7 Time evolution of the NMR gas phase signal intensities of a closed Ru/PVP/H + D_2 sample. The asterisks represent the experimental points. The solid lines visualize the corresponding calculated time evolution. (a) Linear plot and (b) semi-logarithmic plot obtained using the dissociative exchange model. (c) Linear plot and (d) semi-logarithmic plot obtained using the associative exchange model. The plot parameters are assembled in Tables 1 and 2. We note that the dissociative exchange model predicts the release only of H_2 in the early stages of the reaction (Fig. 3), and is, therefore, not in agreement with the experiment, in contrast to the associative exchange model.

In Fig. 10 we discuss the simplified associative exchange of eqn (4d) in more detail. After associative adsorption of D_2 on a surface Ru atom the dihydrogen pair might split and transfer a D leading to the formation of a dihydrogen complex in a neighboring site. On the other hand, also a dihydrogen-hydride exchange may occur. After both processes a HD molecule will be released.

Finally, we note that for the Ru/HDA/H + D_2 sample more HD is observed at large reaction times than predicted by either of the two models (Fig. 8b and 9b). A related effect is observed for the Ru/HDA/D + H_2 sample. We assign this finding to a slow H/D exchange between the Ru surface and the CH_2 groups of the HDA ligand, which was observed by ^{2}H solid state NMR before after very long reaction times.[24] That phenomenon is not observed for PVP as ligand (Fig. 7). This exchange proceeds most probably *via* slow C–H ligand activation composed by C–H adsorption on the metal surface and corresponding σ-complex formation as observed for single metal complexes,[38–43] H transfer to Ru and back transfer of D to the ligand. On the other hand, during the re-hydrogenation more gaseous H_2 was consumed and converted into HD at long reaction times, indicating a reverse re-hydrogenation arising not only by the metal surface but also by the ligand HDA *via* the metal surface. However, as this phenomenon was beyond the scope of this study we did not pursue it further.

Discussion of the kinetic simulation parameters

The parameters used to simulate the solid lines in Fig. 8 and 9 were assembled in Table 1 for the dissociative and in Table 2 for the associative exchange model. As we mainly observed only the production of HD, and as the dead-time between exposure of dihydrogen to the nanoparticles and the start of the NMR measurements was at least 8 min, we were not able to determine reliable kinetic isotope effects or fractionation factors. Nevertheless, in the simulation program we took the well-known deviation of the H_2/HD/D_2 equilibrium constant from the statistical value of 4 (see eqn (2)) into account. In a similar way, it is too early to interpret the pseudo-first order rate constants determined as they depend on the exchange model used. According to the TEM results (Fig. 1) there are more Ru nanoparticles in the Ru/HDA samples than in the Ru/PVP samples, and we would have expected a larger rate constant of the HD production in the former. We find that result only in case of the associative, but not in the case of the dissociative exchange model. On the other hand, the exchange kinetics are slow, independent of the exchange model used, and we can not say

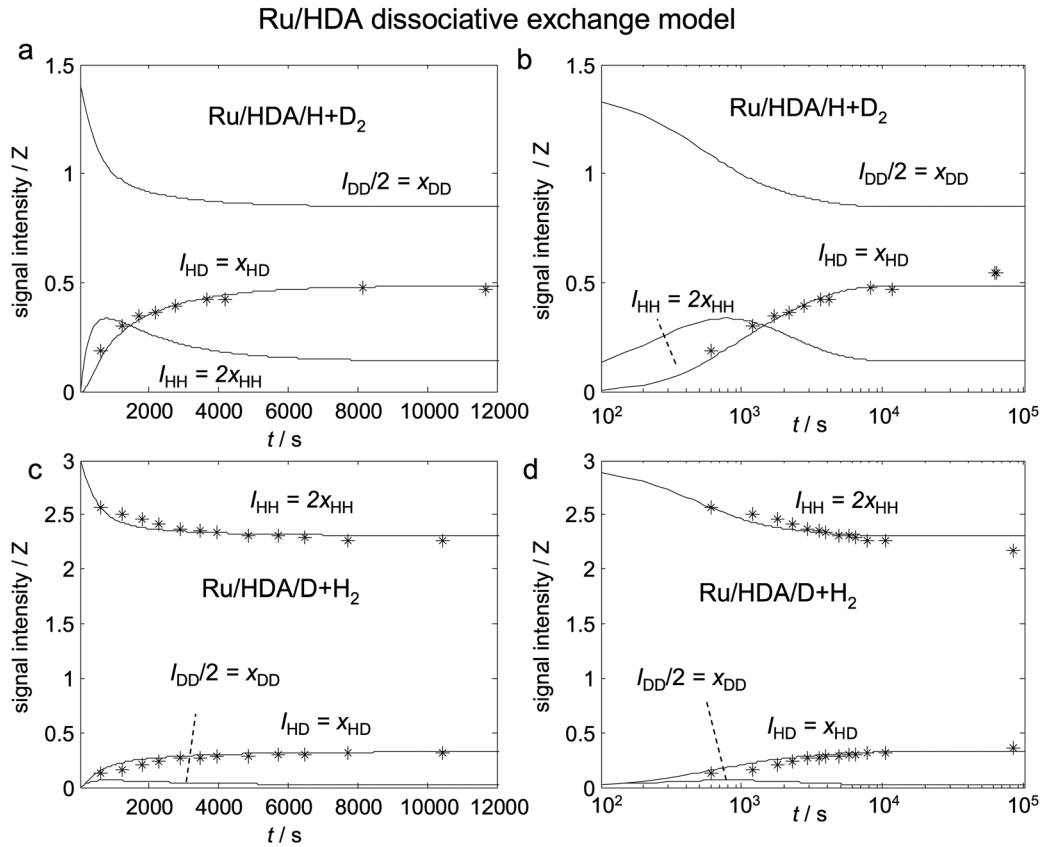

Fig. 8 Time evolution of the NMR gas phase signal intensities of closed Ru/HDA samples. The asterisks represent the experimental points. The solid lines visualize the corresponding calculated time evolution. (a) Linear plot and (b) semi-logarithmic plot obtained for a Ru/HDA/H + D_2 sample using the dissociative exchange model. (a) Linear plot and (b) semi-logarithmic plot obtained for a Ru/HDA/D + H_2 sample using the dissociative exchange model. The plot parameters are assembled in Table 1. We note that the dissociative exchange model predicts the release only of H_2 in the early stages of the reaction (Fig. 3), and is, therefore, not in agreement with the experiment.

Table 1 Overview of parameters used to calculate the gas-surface hydrogen isotope equilibration in terms of the dissociative exchange model of Fig. 3a

Sample/reaction conditions	Variable	Ru/HDA/H + 800 mbar D_2	Ru/HDA/D + 800 mbar H_2	Ru/PVP/H + 800 mbar D_2
Number of isotopologue dihydrogen gas molecules in units of Z	N	1.4	1.5	1.4
Number of ruthenium adsorption sites in units of Z	M	0.8	0.7	0.35
Number of ruthenium adsorption sites mmol	$M \times Z$	0.04	0.035	0.017
HH mole fraction in gas phase at $t = 0$	$x_{HH}(0)$	0	1	0
HD mole fraction in gas phase at $t = 0$	$x_{HD}(0)$	0	0	0
DD mole fraction in gas phase at $t = 0$	$x_{DD}(0)$	1	0	1
Surface deuterium fraction at $t = 0$	$x_D(0)$	0	0.65	0
Pseudo-first order rate constant of HD desorption	k_d^{HD}/s^{-1}	0.0009	0.0009	0.0025
Kinetic HH/HD isotope effect of desorption	$P_1 = \frac{k_d^{HH}}{k_d^{HD}}$	n.d.	n.d.	n.d.
HD/HH isotopic fractionation factor of desorption	ϕ_1	n.d.	n.d.	n.d.

Z = 0.049 mmol. n.d.: not determined, values set to unity.

why. One could conceive H-bond breaking and bond-formation as rate limiting steps, but also diffusion of dihydrogen gases through the organic phases.

On the other hand, the results show that if the dead-time between the start of the reaction and of the experiments can be reduced, and also the gas phase concentration of D_2 could be measured, also kinetic HH/HD/DD isotope effects on the equilibration will become measurable in the future.

Quantification of hydrogen surface sites

In order to quantify the number of hydrides in the Ru surfaces we proceeded as indicated in Table 3. Starting from the

Table 2 Overview of parameters used to calculate the gas-surface hydrogen isotope equilibration in terms of the associative exchange model of Fig. 3b

Sample/reaction conditions	Variable	Ru/HDA/H + 800 mbar D_2	Ru/HDA/D + 800 mbar H_2	Ru/PVP/H + 800 mbar D_2
Number of dihydrogen gas molecules in units of Z	N	1.3	1.43	1.40
Number of ruthenium adsorption sites in units of Z	M	0.9	0.8	0.35
Number of ruthenium adsorption sites mmol	$M \times Z$	0.045	0.04	0.017
HH mole fraction in gas phase at $t = 0$	$x_{HH}(0)$	0	0.93	0
HD mole fraction in gas phase at $t = 0$	$x_{HD}(0)$	0	0.07	0
DD mole fraction in gas phase at $t = 0$	$x_{DD}(0)$	1	0	1
Deuterium fraction on surface at $t = 0$	$x_D(0)$	0	0.4	0
Pseudo-first order rate constant of the reaction $H_2 + D^* \rightarrow H^* + HD$	k^{HHD}/s^{-1}	—	0.00023	0.00045
Pseudo-first order rate constant of the reaction $D_2 + H^* \rightarrow D^* + DH$	k^{DDH}/s^{-1}	0.00023	—	
Kinetic HHD/HDD isotope effect	$P_1 = \frac{k_e^{HHD}}{k_e^{HDD}}$	0.8	0.8	0.8
HHD/HDH isotopic fractionation factor	$\phi_1 = \frac{k_e^{HHD}}{k_e^{HDD}}$	1.8	1.8	1.8

$Z = 0.049$ mmol.

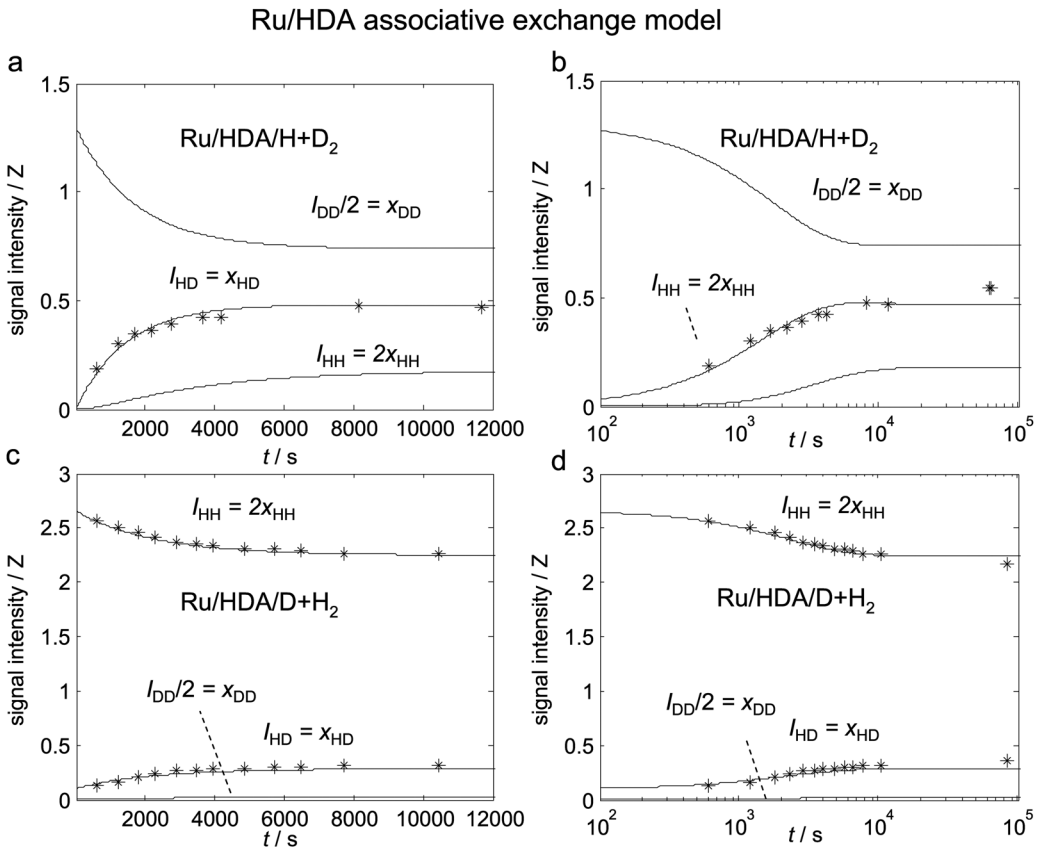

Fig. 9 Time evolution of the NMR gas phase signal intensities of closed Ru/HDA samples. The asterisks represent the experimental points. The solid lines visualize the corresponding calculated time evolution. (a) Linear plot and (b) semi-logarithmic plot obtained for a Ru/HDA/H + D_2 sample using the associative exchange model. (a) Linear plot and (b) semi-logarithmic plot obtained for a Ru/HDA/D + H_2 sample using the associative exchange model. The latter can accommodate the experimental data. The plot parameters are assembled in Table 2.

sample masses, and the weight% of Ru obtained by elemental analysis we obtained the number of Ru atoms (in mmol) of the different samples studied. The fraction of surface Ru has been estimated previously from the particle sizes,[25] leading to the number of surface Ru atoms ($n_{surface\text{-}Ru}$ in mmol). On the other hand, by curve analysis and parameter fitting discussed above we obtained the number of hydrogen adsorption sites M in unit of Z, and by multiplication with Z the corresponding values $M \times Z$ in mmol. Finally, as shown in Table 3, we obtained the number of hydrogen sites per Ru surface atom, $M \times Z/n_{surface\text{-}Ru}$.

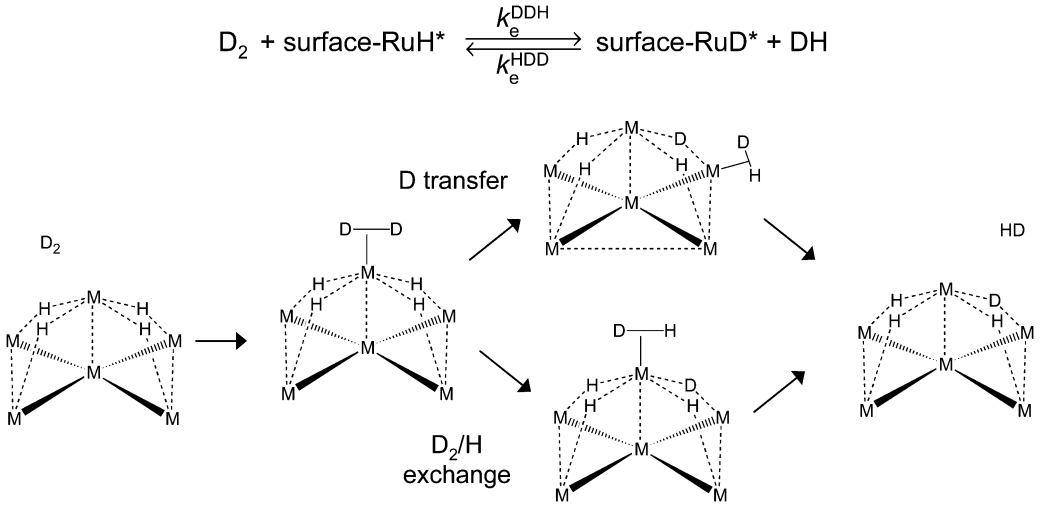

Fig. 10 Possible details of the simplified associative exchange of eqn (4).

Table 3 Quantification of hydrogen adsorption sites

Sample/reaction conditions	Variable	Ru/HDA/H + 800 mbar D_2	Ru/HDA/D + 800 mbar H_2	Ru/PVP/H + 800 mbar D_2
Mass of nanoparticle/mg	m	11	8.4	34
Weight% Ru		53%	53%	7.6%
Amount Ru/mg		5.83	4.45	2.58
Amount Ru/mmol	n_{Ru}	0.058	0.044	0.025
Fraction of surface Ru	$n_{surface\text{-}Ru}/n_{Ru}$	0.52	0.52	0.76
Surface Ru/mMol	$n_{surface\text{-}Ru}$	0.030	0.023	0.019
Number of Ru adsorption sites/mmol dissociative exchange model	$M \times Z$	0.04	0.035	0.017
Number of H sites per Ru surface atoms dissociative exchange model	$M \times Z/n_{surface\text{-}Ru}$	1.3	1.5	0.9
Number of Ru adsorption sites/mmol associative exchange model	$M \times Z$	0.045	0.04	0.017
Number of H sites per Ru surface atoms associative exchange model	$M \times Z/n_{surface\text{-}Ru}$	1.5	1.74	0.89

Z = 0.049 mmol. Atomic mass Ru 101.07.

We obtain similar results for both reaction models. For Ru/HDA we obtain values of about 1.5 and for Ru/PVP values of about 1.

These values are similar to those reported previously[25] by letting 1-octene or norbornene with Ru nanoparticles and measurement of the amounts of the resulting alkanes by gas chromatography and mass spectroscopy. Using that method, 1.2 hydrogen per surface Ru atoms were obtained for Ru/HDA and Ru/PVP.

Under which conditions will the associative hydrogen isotope exchange mechanism dominate?

As our hydrogen isotope gas–metal surface experiments indicate the presence of the associative exchange mechanism the question arises why we do not find the dissociative exchange mechanism as discussed usually.[13] That is the mechanism we and others would have predicted in view of many studies using surface science methods.[3] We tentatively offer here the following explanation. Previous detailed surface science studies of the interaction of hydrogen with clean metal surfaces were carried out mostly at low temperatures and pressures, in contrast to our studies which were done at room temperature and around 1 bar *i.e.* under normal conditions. Under such conditions, not only all terminal hydride sites, bridge $M(\mu^2)$ and $M(\mu^3)$ sites will be occupied, but there might be also dihydrogen complexes of the type $M(\eta^2\text{-H–H})$ present which will increase the number of hydrogens per surface atoms. Whereas previously dihydrogen sites have been observed only in rare cases, *e.g.* Pd surfaces,[7] recently, experimental and computational evidence for H_2 binding to surface Ru atoms has been observed even under conditions of occupied hydride sites.[9,11] Therefore, the associative exchange *via* surface dihydrogen complexes is not in disagreement with previous findings.

Conclusions

We come to the following conclusions:

(i) It is possible to follow the time evolution of exchange of gaseous dihydrogen isotopologues with hydrogen sites in the surface of ligand containing solid Ru-nanoparticles using gas phase ^{1}H NMR spectroscopy in closed samples. That technique allows one to study reactive samples under conditions where the number of hydrogen atoms in the gas phase and the metal nanoparticle surfaces are of comparable size.

(ii) A formalism is developed which allows one to analyze the hydrogen isotope equilibration kinetics and to determine potential kinetic and equilibrium isotope effects of dihydrogen desorption from the Ru-surface as well as the number of surface hydrogen sites. The formalism can be applied in the case of all techniques which are able to determine the concentrations of hydrogen isotopes in the gas phase of a closed system. Two different reaction models were considered, the dissociative and the associative exchange model as illustrated schematically in Fig. 3.

(iii) The technique was applied to analyze the HD production after treatment of hydrogen containing Ru nanoparticles stabilized by polyvinylpyrrolidone (Ru/PVP) and by hexadecylamine (Ru/HDA). Unfortunately, because of a long dead time of several minutes we were not able to determine the initial H_2 production, and could, therefore, not yet determine isotope effects on the equilibration process.

(iv) The results could not be explained in terms of the dissociative exchange model, whereas they were compatible with the associative exchange model proceeding *via* surface dihydrogen complexes.

The relevance of this work for the future use of transition metal nanoparticles in the field of catalysis is that one should think of the possibility that surface sites containing dihydrogen might be the main active surface species responsible for the elementary reaction steps. On the other hand, from a methodological standpoint, it will be useful to extend our approach to the study of colloidal solutions of nanocatalysts. Finally, efforts need to be made in order to reduce the dead-time between the sample preparation and the NMR measurements.

Conflicts of interest

The authors do not declare any conflict of interest.

Appendix

Dissociative exchange

This process consists of dissociative adsorption[3] of dihydrogen isotopes on the metal nanoparticle surfaces, followed by fast surface diffusion and associative desorption. The adsorption/desorption equilibria are given by eqn (3b). Let K_a^{LL} and K_d^{LL} be the equilibrium constants of dihydrogen association and dissociation

$$K_d^{HH} = \frac{k_d^{HH}}{k_a^{HH}} = \frac{1}{K_a^{HH}}, \tag{9a}$$

$$K_d^{HD} = \frac{k_d^{HD}}{k_a^{HD}} = \frac{1}{K_a^{HD}}, \tag{9b}$$

$$K_d^{DD} = \frac{k_d^{DD}}{k_a^{DD}} = \frac{1}{K_a^{DD}}. \tag{9c}$$

We are interested here in the case where the total number of dihydrogen molecules in the gas phase

$$N = n_{H_2} + n_{HD} + n_{D_2} \tag{10}$$

is independent of time, where n_{LL} corresponds to the time-dependent numbers of isotopologue molecules LL = H_2, HD, D_2. Let a given surface contain a fixed number M of such sites. As mentioned above, we consider the high-pressure limit where almost all surface hydrogen sites are occupied. M is then equal to the number of bound hydrogen isotopes and independent of time *i.e.*

$$M = n_{H^*} + n_{D^*} \tag{11}$$

in contrast to the time-dependent numbers n_{LL} and n_{L^*}.

Using eqn (9) one can define the "fractionation factors" of dihydrogen desorption

$$\begin{aligned} \phi_1 &= \frac{K_d^{HD}}{K_d^{HH}} = \frac{K_a^{HH}}{K_a^{HD}} = \frac{n_{HD} n_{H^*}}{2 n_{H_2} n_{D^*}}, \\ \phi_2 &= \frac{K_d^{DD}}{K_d^{HD}} = \frac{K_a^{HD}}{K_a^{DD}} = \frac{2 n_{D_2} n_{H^*}}{n_{HD} n_{D^*}}, \\ \frac{K_d^{DD}}{K_d^{HH}} &= \frac{K_a^{HH}}{K_a^{DD}} = \phi_1 \phi_2 = \frac{n_{D_2} {n_{H^*}}^2}{n_{H_2} {n_{D^*}}^2}. \end{aligned} \tag{12}$$

If $\phi_1 > 1$ or $\phi_2 > 1$, D enriches in the gas phase, and if $\phi_1 < 1$ or $\phi_2 < 1$, D enriches in the surface. However, the two fractionation factors are not independent of each other because of the isotopic equilibrium in the gas phase (eqn (2)). This is because by combination with eqn (9) it follows that

$$K_{gas} = \frac{4\left(K_d^{HD}\right)^2}{K_d^{HH} K_d^{DD}} = 4\frac{\phi_1}{\phi_2} \rightarrow \phi_2 = 4\frac{\phi_1}{K_{gas}}, \tag{13}$$

$$\text{with } \phi_2 = 1.23\phi_1 \text{ at } 298 \text{ K}.$$

We define the kinetic H/D isotope effects of desorption and adsorption as

$$\frac{k_d^{HH}}{k_d^{HD}} = P_1, \quad \frac{k_d^{HD}}{k_d^{DD}} = P_2, \quad \frac{k_d^{HH}}{k_d^{DD}} = P_1 P_2. \tag{14a}$$

As described in the ESI,† we have derived the following set of differential equations describing the time dependence of the variables dihydrogen isotopes in the gas phase and of the surface hydrogens n_{H_2}, n_{HD}, n_{D_2} and n_{D^*} which characterizes the isotopic equilibration process *via* dissociative exchange

$$\frac{dn_{H_2}}{dt} = \frac{k_d^{HH}}{M}\left(-n_{H_2}\frac{{n_{H^*}}^2 + 2{P_1}^{-1} n_{H^*} n_{D^*} + {P_1}^{-1}{P_2}^{-1}{n_{D^*}}^2}{n_{H_2} + \frac{n_{HD}}{\phi_1 P_1} + \frac{n_{D_2}}{\phi_1\phi_2 P_1 P_2}} + {n_{H^*}}^2\right), \tag{15a}$$

$$\frac{dn_{HD}}{dt} = \frac{k_d^{HH}}{M}\left(-n_{HD}\frac{{n_{H^*}}^2 + 2{P_1}^{-1} n_{H^*} n_{D^*} + {P_1}^{-1}{P_2}^{-1}{n_{D^*}}^2}{\phi_1 P_1 n_{H_2} + n_{HD} + \frac{n_{D_2}}{\phi_2 P_2}} + 2{P_1}^{-1} n_{H^*} n_{D^*}\right), \tag{15b}$$

$$\frac{dn_{D_2}}{dt} = -\frac{k_d^{HH}}{M}\left(n_{D_2}\frac{{n_{H^*}}^2 + 2{P_1}^{-1}n_{H^*}n_{D^*} + {P_1}^{-1}{P_2}^{-1}{n_{D^*}}^2}{\phi_1\phi_2 P_1 P_2 n_{H_2} + \phi_2 P_2 n_{HD} + n_{D_2}} + {P_1}^{-1}{P_2}^{-1}{n_{D^*}}^2\right), \quad (15c)$$

$$\frac{dn_{H^*}}{dt} = -2\frac{dn_{H_2}}{dt} - \frac{dn_{HD}}{dt}. \quad (15d)$$

$$\frac{dn_{D^*}}{dt} = -\frac{dn_{HD}}{dt} - 2\frac{dn_{D_2}}{dt}. \quad (15e)$$

The parameters needed to simulate a given kinetic run are the total number N of isotopologue dihydrogen molecules in the gas phase, the number M of hydrogen sites in the solid, the number of species $n_{HH}(0)$, $n_{HD}(0)$ and $n_{D^*}(0)$ at t = 0, the pseudo-first rate constant of desorption k_d^{HH} (or alternatively k_d^{HD} or k_d^{DD}), the kinetic isotope effects P_1 and P_2 of desorption and the isotopic fractionation factor ϕ_1. Applications are presented in Fig. 7 and 8.

Associative exchange

In this model, we assume that gaseous dihydrogen molecules can bind to the surface and exchange directly hydrogen isotopes with a neighboring bound, releasing again a dihydrogen molecule as illustrated in Fig. 3b and in eqn (4). The time dependence of different isotopic species is given by

$$\frac{dn_{D_2}}{dt} = -k_e^{DDH}n_{DD}n_{H^*} + k_e^{HDD}n_{HD}n_{D^*}, \quad (16a)$$

$$\frac{dn_{HD}}{dt} = -k_e^{DHH}n_{HD}n_{H^*} - k_e^{HDD}n_{HD}n_{D^*} + k^{DDH}n_{DD}n_{H^*} + k^{HHD}n_{HH}n_{D^*}, \quad (16b)$$

$$\frac{dn_{H_2}}{dt} = -k_e^{HHD}n_{HH}n_{D^*} + k_e^{DHH}n_{HD}n_{H^*}, \quad (16c)$$

$$\frac{dn_{D^*}}{dt} = -\frac{dn_{H^*}}{dt} = k_e^{DDH}n_{DD}n_{H^*} - k_e^{HDD}n_{HD}n_{D^*} + k_e^{DHH}n_{HD}n_{H^*} - k_e^{HHD}n_{HH}n_{D^*}. \quad (16d)$$

At equilibrium

$$\frac{dn_{D_2}^{\infty}}{dt} = 0 = k_e^{DDH}n_{DD}^{\infty}n_{H^*}^{\infty} + k_e^{HDD}n_{HD}^{\infty}n_{D^*}^{\infty}, \quad (17a)$$

$$\frac{dn_{HD}}{dt} = 0 = -k_e^{DHH}n_{HD}n_{H^*} - k_e^{HDD}n_{HD}n_{D^*} + k^{DDH}n_{DD}n_{H^*} + k^{HHD}n_{HH}n_{D^*}, \quad (17b)$$

$$\frac{dn_{H_2}}{dt} = 0 = -k_e^{HHD}n_{HH}n_{D^*} + k_e^{DHH}n_{HD}n_{H^*}, \quad (17c)$$

$$\frac{dn_{D^*}}{dt} = 0 = -\frac{dn_{H^*}}{dt} = k_e^{DDH}n_{DD}n_{H^*} - k_e^{HDD}n_{HD}n_{D^*} + k_e^{DHH}n_{HD}n_{H^*} - k_e^{HHD}n_{HH}n_{D^*}, \quad (17d)$$

from which it follows that

$$\frac{k_e^{HHD}}{k_e^{DHH}} = \frac{n_{HD}^{\infty}n_{H^*}^{\infty}}{n_{HH}^{\infty}n_{D^*}^{\infty}} = \phi_1 \quad \text{and} \quad \frac{k_e^{HDD}}{k_e^{DDH}} = \frac{n_{DD}^{\infty}n_{H^*}^{\infty}}{n_{HD}^{\infty}n_{D^*}^{\infty}} = \phi_2. \quad (18)$$

ϕ_1 and ϕ_2 are fractionation factors which represent the equilibrium constants of the isotopic reactions

$$H_2 + D^* + \underset{k_e^{DHH}}{\overset{k_e^{HHD}}{\rightleftharpoons}} HD + H^*, \quad (19a)$$

$$HD + D^* + \underset{k_e^{DDH}}{\overset{k_e^{HDD}}{\rightleftharpoons}} D_2 + H^*. \quad (19b)$$

Please note that these are not the same quantities as those defined in the previous section, but in a similar way they are not independent of each other because of the isotopic equilibrium in the gas phase (eqn (1)). By combination of eqn (2) and (18) it follows that

$$K_{gas} = K = \frac{n_{HD}^{\infty}n_{HD}^{\infty}}{n_{HH}^{\infty}n_{DD}^{\infty}} = \frac{k_e^{HHD}k_e^{DDH}}{k_e^{DHH}k_e^{HDD}} = \frac{\phi_1}{\phi_2}. \quad (20)$$

Let us define the kinetic isotope effect

$$P_1 = \frac{k_e^{HHD}}{k_e^{HDD}}, \quad (21)$$

which corresponds to the rate constant ratio of the H transfer from H_2 to D* and of the D transfer from HD to D*. Using eqn (18) we can then express all rate constants in eqn (21) as

$$k_e^{HDD} = \frac{k_e^{HHD}}{P_1}, \quad k_e^{DHH} = \frac{k_e^{HHD}}{\phi_1}, \quad k_e^{DDH} = \frac{k_e^{HDD}}{\phi_2} = \frac{Kk_e^{HDD}}{\phi_1} = \frac{Kk_e^{HHD}}{P_1\phi_1}. \quad (22)$$

As shown in the ESI† it follows then from eqn (16) and (17) that

$$\frac{dn_{D_2}}{dt} = k_e^{HHD}\left\{-\frac{K}{P_1\phi_1}\left(n_{DD}n_{H^*} - n_{DD}^{\infty}n_{H^*}^{\infty}\right) + \frac{1}{P_1}\left(n_{HD}n_{D^*} - n_{HD}^{\infty}n_{D^*}^{\infty}\right)\right\}, \quad (23a)$$

$$\frac{dn_{HD}}{dt} = k_e^{HHD}\left\{-\frac{1}{\phi_1}\left(n_{HD}n_{H^*} - n_{HD}^{\infty}n_{H^*}^{\infty}\right) - \frac{1}{P_1}\left(n_{HD}n_{D^*} - n_{HD}^{\infty}n_{D^*}^{\infty}\right) + \frac{K}{P_1\phi_1}\left(n_{DD}n_{H^*} - n_{DD}^{\infty}n_{H^*}^{\infty}\right) + \left(n_{HH}n_{D^*} - n_{HH}^{\infty}n_{D^*}^{\infty}\right)\right\}, \quad (23b)$$

$$\frac{dn_{H_2}}{dt} = k_e^{HHD}\left\{-\left(n_{HH}n_{D^*} - n_{HH}^{\infty}n_{D^*}^{\infty}\right) + \frac{1}{\phi_1}\left(n_{HD}n_{H^*} - n_{HD}^{\infty}n_{H^*}^{\infty}\right)\right\}, \quad (23c)$$

$$\frac{dn_{D^*}}{dt} = -\frac{dn_{H^*}}{dt} = k_e^{HHD}\left\{\frac{K}{P_1\phi_1}\left(n_{DD}n_{H^*} - n_{DD}^{\infty}n_{H^*}^{\infty}\right) - \frac{1}{P_1}\left(n_{HD}n_{D^*} - n_{HD}^{\infty}n_{D^*}^{\infty}\right) + \frac{1}{\phi_1}\left(n_{HD}n_{H^*} - n_{HD}^{\infty}n_{H^*}^{\infty}\right) - \left(n_{HH}n_{D^*} - n_{HH}^{\infty}n_{D^*}^{\infty}\right)\right\}. \quad (23d)$$

The time dependence of the concentrations of the different species can be calculated as a function of the parameters k_e^{HHD}, P_1, ϕ_1, and of the initial sample composition. In order to solve eqn (23) numerically, a MATLAB program was written where the quantities on the left sides of eqn (23) were calculated as a function of time using sufficiently small time intervals from the corresponding quantities at $t = 0$. The equilibrium values in eqn (23) can be calculated from the initial sample conditions as shown in the ESI.† Applications are presented in Fig. 7 and 9.

Acknowledgements

This work has been supported by the CNRS, Toulouse, the Deutsche Forschungsgemeinschaft ''Monitoring catalytic reactions on Nanoparticles by solid state NMR: a joint experimental and theoretical approach'', BU 911/19-1/2, Bonn, and the Agence National de Recherche, Paris.

References

1 (*a*) R. Döll, G. Lauth, E. Schwarz and K. Christmann, The Adsorption of Hydrogen on a Ru(10−10) Surface, *J. Chem. Phys.*, 1989, **91**, 3729–3743; (*b*) L. Hammer, K. Heinz, K. Bedürftig, U. Muschiol, K. Christmann, A. P. Seitsonen, H. Bludau and H. Over, Anomalous hydrogen adsorption sites found for the c(2 × 2)-3H phases formed on the Re(10−10) and Ru(10−10) surfaces, *J. Chem. Phys.*, 1998, **108**, 8671–8679; (*c*) K. Christmann, Hydrogen Transfer on Metal Surfaces, in *Hydrogen Transfer*, ed. J. T. Hynes, H. H. Limbach, J. Klinman and R. L. Schowen, Wiley-VCH, Weinheim, Germany, 2006, ch. 25, vol. 1, pp. 751–786.

2 (*a*) P. Feulner and D. Menzel, The adsorption of hydrogen on ruthenium (001): Adsorption states, dipole moments and kinetics of adsorption and desorption, *Surf. Sci.*, 1985, **154**, 465–488; (*b*) M. Y. Chou and J. R. Chelikowsky, First-principles study of hydrogen adsorption on Ru(0001): Possible occupation of subsurface sites, *Phys. Rev. Lett.*, 1987, **59**, 1737–1740; (*c*) P. J. Feibelman, J. E. Houston, H. L. Davis and D. G. O'Neill, Relaxation of the clean, Cu- and H-covered Ru(0001) surface, *Surf. Sci.*, 1994, **302**, 81–92; (*d*) P. Hoffmann and D. Menzel, Synchrotron radiation studies of hydrogen adsorption on Ru(001), *Surf. Sci.*, 1985, **152**, 382–391; (*e*) M. Lindroos, H. Pfnür and D. Menzel, Investigation of a disordered adsorption system by electron reflection: H/Ru(001) at intermediate coverages, *Surf. Sci.*, 1987, **192**, 421–437; (*f*) M. Sokolowski, T. Koch and H. Pfnür, Ordered structures and phase diagram of atomic hydrogen chemisorbed on ruthenium(001), *Surf. Sci.*, 1991, **243**, 261–272.

3 K. Christmann, Adsorption of Hydrogen, in *Surface and Interface Science*, ed. K. Wandelt, Wiley-VCH, Weinheim, Germany, 2016, ch. 36, vol. 5 Solid–Gas Interfaces I, pp. 255–356, DOI: 10.1002/9783527680573.ch36.

4 T. Mitsui, M. K. Rose, E. Fomin, D. F. Ogletree and M. Salmeron, Dissociative hydrogen adsorption on palladium requires aggregates of three or more vacancies, *Nature*, 2003, **422**, 705–707.

5 A. Auerbach, K. F. Freed and R. Gomer, Anomalous isotope dependence of hydrogen diffusion rates on tungsten (110) surfaces: Implications for lattice–hydrogen interactions, *J. Chem. Phys.*, 1987, **86**, 2356–2361.

6 (*a*) D. N. Denzler, C. Frischkorn, C. Hess, M. Wolf and G. Ertl, Electronic Excitation and Dynamic Promotion of a Surface Reaction, *Phys. Rev. Lett.*, 2003, **91**, 226102; (*b*) D. N. Denzler, C. Frischkorn, M. Wolf and G. Ertl, Surface Femtochemistry: Associative Desorption of Hydrogen from Ru(001) Induced by Electronic Excitations, *J. Phys. Chem. B*, 2004, **108**, 14503–14510.

7 P. K. Schmidt, K. Christmann, G. Kresse, J. Hafner, M. Lischka and A. Groß, Coexistence of atomic and molecular chemisorption states: H_2/Pd(210), *Phys. Rev. Lett.*, 2001, **87**, 096103.

8 H. A. Aleksandrov, S. M. Kozlov, S. Schauermann, G. N. Vayssilov and K. M. Neyman, How Absorbed Hydrogen Affects the Catalytic Activity of Transition Metals, *Angew. Chem., Int. Ed.*, 2014, **53**, 13371–13375.

9 D. Bumüller, A. S. Hehn, E. Waldt, R. Ahlrichs, M. M. Kappes and D. Schooss, Ruthenium Cluster Structure Change Induced by Hydrogen Adsorption: Ru_{19}, *J. Phys. Chem. C*, 2017, **121**, 10645–10652.

10 C. P. O'Brien, K. H. Dostert, M. Hollerer, C. Stiehler, F. Calaza, S. Schauermann, S. Shaikhutdinov, M. Sterrer and H. J. Freund, Supports and modified nano-particles for designing model catalysts, *Faraday Discuss.*, 2016, **188**, 309–321.

11 L. Cusinato, L. M. Martínez–Prieto, B. Chaudret, I. del Rosal and R. Poteau, Theoretical characterization of the surface composition of ruthenium nanoparticles in equilibrium with syngas, *Nanoscale*, 2016, **8**, 10974–10992.

12 M. Benkhaled, C. Descorme, D. Duprez, S. Morin, C. Thomazeau and D. Uzio, Study of hydrogen surface mobility and hydrogenation reactions over alumina-supported palladium catalysts, *Appl. Catal., A*, 2008, **346**, 36–43.

13 C. Fernández, N. Bion, E. M. Gaigneaux, D. Duprez and P. Ruiz, Kinetics of hydrogen adsorption and mobility on Ru nanoparticles supported on alumina: Effects on the catalytic mechanism of ammonia synthesis, *J. Catal.*, 2016, **344**, 16–28.

14 A. Mirich, T. Hoette Miller, E. Klotz and B. Mattson, Heterogeneous catalysis: deuterium exchange reactions of hydrogen and methane, *J. Chem. Educ.*, 2015, **92**, 2087–2093.

15 M. T. Reetz, R. Breinbauer, P. Wedemann and P. Binger, Nanostructured nickel-clusters as catalysts in [3+2] cycloaddition reactions, *Tetrahedron*, 1998, **54**, 1223–1240.

16 *Nanoparticles and Catalysis*, ed. D. Astruc, Wiley-VCH, Weinheim, Germany, 2008.

17 (*a*) L. N. Lewis, Chemical catalysis by colloids and clusters, *Chem. Rev.*, 1993, **93**, 2693–2730; (*b*) J. D. Aiken III and R. G. Finke, A review of modern transition-metal nanoclusters: their synthesis, characterization, and applications in catalysis, *J. Mol. Catal. A: Chem.*, 1999, **145**, 1–44; (*c*) M. A. El-Sayed, Some Interesting Properties of Metals Confined in Time and Nanometer Space of Different Shapes, *Acc. Chem. Res.*, 2001, **34**, 257–264; (*d*) H. Bönnemann and R. M. Richards, Nanoscopic Metal Particles – Synthetic Methods and Potential Applications, *Eur. J. Inorg. Chem.*, 2001, 2455–2480; (*e*) A. Roucoux, J. Schulz and H. Patin, Reduced Transition Metal Colloids: A Novel Family of Reusable Catalysts?, *Chem. Rev.*, 2002, **102**, 3757–3778; (*f*) J. A. Widegren and R. G. Finke, A review of soluble transition–metal nanoclusters as arene hydrogenation catalysts, *J. Mol. Catal. A: Chem.*, 2003, **191**, 187–207.

18 (*a*) M. Studer, H. U. Blaser and C. Exner, Enantioselective Hydrogenation Using Heterogeneous Modified Catalysts: An Update, *Adv. Synth. Catal.*, 2003, **345**, 45–65; (*b*) S. Jansat, M. Gomez, K. Philippot, G. Muller, E. Guiu, C. Claver, S. Castillon and B. Chaudret, A Case for Enantioselective Allylic Alkylation Catalyzed by Palladium Nanoparticles, *J. Am. Chem. Soc.*, 2004, **126**, 1592–1593.

19 G. Schmid, M. Bäumle, M. Geerkens, I. Heim, C. Osemann and T. Sawitowski, Current and future applications of nanoclusters, *Chem. Soc. Rev.*, 1999, **28**, 179–185.

20 (*a*) G. Schmid, *Clusters and colloids, from theory to applications*, VCH, Weinheim, 1994; (*b*) K. J. Klabunde and G. Cardenas-Trivino, in *Active Metals: Preparation, Characterization, Applications*, ed. A. Fürstner, VCH, Weinheim, 1996, pp. 237–277; (*c*) K. Philippot and B. Chaudret, Organometallic approach to the synthesis and surface reactivity of noble metal nanoparticles, *C. R. Chim.*, 2003, **6**, 1019–1034, and references therein.

21 (*a*) J. S. Bradley, E. W. Hill, S. Behal, C. Klein, B. Chaudret and A. Duteil, Preparation and characterization of organosols of monodispersed nanoscale palladium. Particle size effects in the binding geometry of adsorbed carbon monoxide, *Chem. Mater.*, 1992, **4**, 1234–1239; (*b*) D. de Caro and J. S. Bradley, Surface Spectroscopic Study of Carbon Monoxide Adsorption on Nanoscale Nickel Colloids Prepared from a Zerovalent Organometallic Precursor, *Langmuir*, 1997, **13**, 3067–3069; (*c*) D. de Caro and J. S. Bradley, Surface Chemistry of Colloidal Platinum: Vibrational Coupling in the Infrared Spectrum of CO Adsorbed on Colloidal Platinum in Liquid Dispersion, *Langmuir*, 1998, **14**, 245–247.

22 C. Pan, K. Pelzer, K. Philippot, B. Chaudret, F. Dassenoy, P. Lecante and M. J. Casanove, Ligand-Stabilized Ruthenium Nanoparticles: Synthesis, Organization, and Dynamics, *J. Am. Chem. Soc.*, 2001, **123**, 7584–7593.

23 (*a*) G. Pieters, C. Taglang, E. Bonnefille, T. Gutmann, C. Puente, J. C. Berthet, C. Dugave, B. Chaudret and B. Rousseau, Regioselective and Stereospecific Deuteration of Bioactive Aza Compounds by the Use of Ruthenium Nanoparticles, *Angew. Chem., Int. Ed.*, 2014, **53**, 230–234; (*b*) C. Taglang, L. M. Martínez-Prieto, I. Del Rosal, L. Maron, R. Poteau, K. Philippot, B. Chaudret, S. Perato, A. Sam Lone, C. Puente, C. Dugave, B. Rousseau and G. Pieters, Enantiospecific C–H Activation Using Ruthenium Nanocatalysts, *Angew. Chem., Int. Ed.*, 2015, **54**, 10474–10477.

24 T. Pery, K. Pelzer, G. Buntkowsky, K. Philippot, H. H. Limbach and B. Chaudret, Direct NMR Evidence for the Presence of Mobile Surface Hydrides on Ruthenium Nanoparticles, *ChemPhysChem*, 2005, **6**, 605–607.

25 J. García-Antón, M. R. Axet, S. Jansat, K. Philippot, B. Chaudret, T. Pery, G. Buntkowsky and H. H. Limbach, Reactions of olefins with novel ruthenium hydride nanoparticles: NMR characterization, hydride titration and room temperature C–C activation, *Angew. Chem., Int. Ed.*, 2008, **47**, 2074–2078.

26 T. Gutmann, B. Walaszek, Y. Xu, M. Wächtler, A. Grünberg, I. del Rosal, R. Poteau, R. Axet, G. Lavigne, B. Chaudret, H. H. Limbach and G. Buntkowsky, Hydrido-ruthenium cluster complexes as models for reactive surface hydrogen species of ruthenium nanoparticles-Solid-state ^{2}H NMR and quantum chemical calculations, *J. Am. Chem. Soc.*, 2010, **132**, 11759–11767.

27 T. Gutmann, I. del Rosal, B. Chaudret, R. Poteau, H. H. Limbach and G. Buntkowsky, From Molecular Complexes to Complex Metallic Nanostructures-^{2}H Solid-State NMR Studies of Ruthenium-Containing Hydrogenation Catalysts, *ChemPhysChem*, 2013, **14**, 3026–3033.

28 I. del Rosal, T. Gutman, B. Walaszek, I. C. Gerber, B. Chaudret, H. H. Limbach, G. Buntkowsky and R. Poteau, NMR calculations on polynuclear transition metal complexes: on the influence of local symmetry, *Phys. Chem. Chem. Phys.*, 2011, **13**, 20199–20207.

29 (*a*) G. J. Kubas, R. R. Ryan, B. I. Swanson, P. J. Vergamini and H. J. Wasserman, Characterization of the First Examples of Isolable Molecular Hydrogen Complexes, $M(CO)_3(PR_3)_2(H_2)$(M = Mo, W; R = Cy, i-Pr). Evidence for a Side-on Bonded H_2 Ligand, *J. Am. Chem. Soc.*, 1984, **106**, 452–454; (*b*) H. H. Limbach, S. Ulrich, G. Buntkowsky, S. Gründemann, S. Sabo-Etienne, B. Chaudret, G. J. Kubas and J. Eckert, NMR and INS Line Shapes of Transition Metal Hydrides in the Presence of Coherent and Incoherent Dihydrogen Exchange, *J. Am. Chem. Soc.*, 1998, **120**, 7929–7943.

30 F. Wehrmann, T. P. Fong, R. H. Morris, H. H. Limbach and G. Buntkowsky, Coherent D_2 Rotational Tunneling and Incoherent D_2 Dynamics in a Solid Non-classical RuD_2 Complex studied by ^{2}H Solid State NMR Spectroscopy, *Phys. Chem. Chem. Phys.*, 1999, **1**, 4033–4041.

31 J. Matthes, T. Pery, S. Gründemann, G. Buntkowsky, S. Sabo-Etienne, B. Chaudret and H. H. Limbach, Bridging the Gap between Homogeneous and Heterogeneous Catalysis: ortho/para-H_2 Conversion, Hydrogen Isotope Scrambling and Hydrogenation of Olefins by $Ir(CO)Cl(PPh_3)_2$, *J. Am. Chem. Soc.*, 2004, **126**, 8366–8367.

32 A. Abragam, *The Principles of nuclear Magnetism*, Oxford University Press, London, 1961, ch. VIII.

33 H. C. Urey, The thermodynamic properties of isotopic substances, *J. Chem. Soc.*, 1947, 562–581.
34 O. Thompson and O. A. Schaeffer, Radiation Induced Equilibrium of Hydrogen-Deuterium Mixtures, *J. Chem. Phys.*, 1955, **23**, 759–760.
35 I. Chorkendorff and J. W. Niemantsverdriet, *Concepts of Modern Catalysis and Kinetics*, Wiley-VCH, Weinheim, 2003.
36 H. Sabzyan, F. R. W. McCourt and W. P. Power, Experimental and theoretical study of proton spin–lattice relaxation in H_2–Ar gas mixtures: Critical examination of the XC(fit) potential energy surface, *J. Chem. Phys.*, 2004, **120**, 4306–4315.
37 E. L. Hahn, Spin Echoes, *Phys. Rev.*, 1950, **80**, 580–594.
38 W. D. Jones, Isotope Effects in C–H Bond Activation Reactions by Transition Metals, *Acc. Chem. Res.*, 2003, **36**, 140–146.
39 (*a*) K. E. Janak and G. Parkin, Temperature-Dependent Transitions between Normal and Inverse Equilibrium Isotope Effects for Coordination and Oxidative Addition of C–H and H–H Bonds to a Transition Metal Center, *J. Am. Chem. Soc.*, 2003, **125**, 6889–6891; (*b*) K. E. Janak and G. Parkin, Experimental Evidence for a Temperature Dependent Transition between Normal and Inverse Equilibrium Isotope Effects for Oxidative Addition of H2 to $Ir(PMe_2Ph)_2(CO)Cl$, *J. Am. Chem. Soc.*, 2003, **125**, 13219–13224.
40 S. Geftakis and G. E. Ball, Direct Observation of a Transition Metal Alkane Complex, $CpRe(CO)_2$(cyclopentane), Using NMR Spectroscopy, *J. Am. Chem. Soc.*, 1998, **120**, 9953–9954.
41 R. H. Schultz, A. A. Bengali, B. H. Weiller, E. P. Wasserman, K. R. Kyle, C. B. Moore and R. G. Bergman, IR Flash Kinetic Spectroscopy of C–H Bond Activation of Cyclohexane-d_0 and -d_{12} by $Cp^*Rh(CO)_2$ in Liquid Rare Gases: Kinetics, Thermodynamics, and Unusual Isotope Effect, *J. Am. Chem. Soc.*, 1994, **116**, 7369–7377.
42 M. Lersch and M. Tilset, Mechanistic Aspects of C–H Activation by Pt Complexes, *Chem. Rev.*, 2005, **105**, 2471–2526.
43 A. L. Pitts, A. Wriglesworth, X. Z. Sun, J. A. Calladine, S. D. Zarić, M. W. George and M. B. Hall, Carbon–hydrogen activation of cycloalkanes by cyclopentadienylcarbonylrhodium–A Lifetime Enigma, *J. Am. Chem. Soc.*, 2014, **136**, 8614–8625.

